ELSEVIER

Journal of Alloys and Compounds 404–406 (2005) 405–408

Journal of ALLOYS AND COMPOUNDS

www.elsevier.com/locate/jallcom

Preliminary results of hydrogen adsorption and SAXS modelling of mesoporous silica: MCM-41

D.A. Sheppard, C.F. Maitland, C.E. Buckley*

Department of Applied Physics, Curtin University of Technology, GPO Box U 1987, Perth, WA, Australia

Received 1 June 2004; received in revised form 23 September 2004; accepted 28 September 2004
Available online 14 July 2005

Abstract

A sample of MCM-41 at 77 K was shown to reversibly absorb 1.6 excess wt% of hydrogen at ∼3.5 MPa. Though the excess hydrogen adsorption peaked, the total gravimetric wt% of hydrogen adsorption continued to increase and reached a value of 2.7 wt% by ∼4.5 MPa. The correlation function has been used here for the first time in an attempt to determine the average pore size, distance between the pores and an estimate of the wall thickness by modelling the entire small angle X-ray scattering (SAXS) curve of the MCM-41 sample. At this stage of the model development, only a lower limit on the average pore size can be determined.

Keywords: Hydrogen storage material; Amorphous materials

1. Introduction

Hydrogen storage is currently an active area of research. Numerous materials are being considered for hydrogen storage including metal and complex metal hydrides, various forms of carbons, zeolites and metal organic frameworks [1]. MCM-41 is a silica-based material with a regular hexagonal array of cylindrical pores. The pore walls are amorphous but the regular array of cylindrical mesopores generates diffraction peaks at low scattering angles [2]. Accurate information about the pore structure must be known before its influence on hydrogen adsorption can be determined. Consequently we aim to develop a technique using SAXS to characterise the pore structure of MCM-41. Here we present the preliminary results for the hydrogen adsorption on an unmodified sample of MCM-41 produced using cetyltrimethyl ammonium bromide and structural information determined using our method for analyzing SAXS data.

2. Experimental procedures

The reagents for the purely siliceous MCM-41 were: sodium silicate solution (Sigma—Aldrich, 27% SiO_2, 59% H_2O, 14% NaOH): cetyltrimethyl ammonium bromide (CTAB) also from Sigma–Aldrich: 98% reagent grade H_2SO_4. The typical molar composition for a sample was $1SiO_2$:0.26CTAB:$0.09H_2SO_4$:$275.6H_2O$. After mixing, the pH of the solution was reduced to 10 with the addition of 1 M sulphuric acid. The final solution was aged statically in a polypropylene bottle at 70 °C. Each day the pH of the gel was reduced to 10 under gentle stirring with a total aging time of 4 days. Calcination was performed over night in a muffle furnace at 500 °C. Hydrogen adsorption experiments were performed on a volumetric apparatus built at Curtin University. All samples were evacuated at 200 °C overnight prior to H_2 adsorption. The compressibility of hydrogen was accounted for by using the modified van der Waals equation of Hemmes et al. [3] following the method of McLennan and Gray [4]. The SAXS patterns were measured with the NanoSTAR SAXS instrument at Curtin University. The powder samples were mounted between thin polymer

* Corresponding author. Tel.: +61 8 9266 3532; fax: +61 8 9266 2377.
E-mail address: c.buckley@curtin.edu.au (C.E. Buckley).

0925-8388/$ – see front matter © 2005 Elsevier B.V. All rights reserved.
doi:10.1016/j.jallcom.2004.09.089

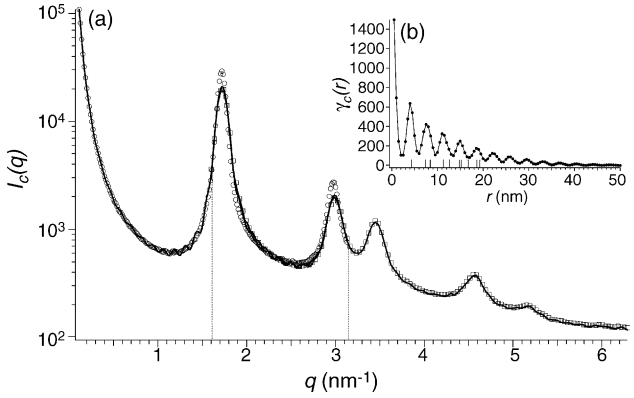

Fig. 1. (a) Experimental cross-section intensity, open circles and squares represent data recorded at sample detector distances of 65.0 and 22.8 cm, respectively. The solid line represents the model cross-section intensity calculated by GNOM. The two experimental data sets overlap in the region bounded by the dashed lines. (b) Cross-section correlation function as calculated by GNOM from the two experimental data sets. Small vertical bars show the first ten nearest neighbour distances for a hexagonal lattice with $a = 4.2$ nm. *Y*-axes are in arbitrary units.

films during these measurements. Data was recorded at two sample-detector distances, 22.8 and 65.0 cm, using a wavelength, λ of 0.15418 nm (Cu Kα). Since two sample-detector distances were used, the scattered intensity consisted of two data sets that overlapped in the q-range displayed in Fig. 1a. Scattered photons were counted with a 2D multiwire detector. The raw data had the background subtracted and was radially averaged. Resulting intensities, after discarding low q data points affected by the beam stop, spanned a q-range between 0.11 and 8.45 nm^{-1} ($q = 4\pi \sin\theta/\lambda$, where θ is half the scattering angle). The instrument was calibrated using silver-behenate, which produces low-angle diffraction peaks at known positions [5]. Samples for TEM were grain mounted and TEM images were recorded on a Jeol 2011 operating at 200 kV.

2.1. Method of SAXS analysis

Small-angle X-ray scattering arises due to differences in the electron density of inhomogeneities that are between one and several hundred nm in size [6]. For rod-like particles with a cross-section electron density distribution that does not vary along the long axis, the intensity can be separated into two components:

$$I(q) = Cq^{-1}I_c(q) \quad (1)$$

This equation is valid for $q > 2\pi/L$, where L is length of the rod [6], $I_c(q)$ the cross-section intensity, and C is a constant that takes into account such things as sample thickness, incident beam flux etc. This equation is also valid for rods that are slightly bending [7]. Transmission electron microscope (TEM) images have shown that within our sample of MCM-41 there are ordered 'domains', analogous to crystallites, in which all pores lie on a single hexagonal lattice. The micron-sized powder grains consist of a number of these domains packed together in different orientations. Our analysis is based on the assumption that the electron density is slowly varying within these domains in the direction of the long axis of the pores. In this case the cross-section intensity would be dependent on the electron density distribution of the cross-section, perpendicular to the long axis of the pores, within each of the domains. For the use of Eq. (1) to be valid the length L of all the domains would need to be greater than $2\pi/q_{min} = 55$ nm. TEM images have shown that most of the domains are longer than 55 nm and some exceed several hundred nanometres in length. The pore size and spacing determine the cross-sectional structure of the domains, therefore the cross-section intensity contains the information of interest. The cross-section intensity is related to the cross-section correlation function (CF) $\gamma_c(r)$ as follows [6]:

$$I_c(q) = \int_0^D r\gamma_c(r)J_0(qr)\mathrm{d}r \quad (2)$$

where r is a distance that joins two points within the cross-section, D the maximum dimension of the cross-section, $J_0(qr)$ the Bessel function of zero order and $\gamma_c(r)$ gives a probabilistic description of the electron density correlations within the cross-section.

To extract the cross-section CF the GNOM program [8] was used. It employs the Tikhonov regularisation method [9] to solve the ill-posed problem of determining $\gamma_c(r)$ from $I_c(q)$. The maximum dimension D must be estimated when using this method, which was approximated from the full width at half maximum Δq of the d_{10} peak (see first peak in Fig. 1a) in $I_c(q)$ ($D \approx 2\pi/\Delta q \approx 50$ nm). TEM images show that on average the maximum dimension of the cross-section of the domains exceeded the calculated D. Thus, we conclude that the calculated D is dependent on the largest distance over which the domains are ordered and instrumental broadening. It is assumed that electron density correlations over distances greater than D are not significant in the sample and/or they cannot be measured with the current experimental setup. Using the calculated D, any $\gamma_c(r)$ determined from modelling the experimental data would be expected to approximately equal zero for $r > D$. The behaviour of $\gamma_c(r)$ at large r is not of interest, therefore any loss of information introduced by the above assumption is not significant to the present study. The two data sets, recorded at different sample-detector distances, were modelled simultaneously by GNOM over the q-range $0.11 \leq q(\mathrm{nm}^{-1}) \leq 6.29$.

3. Experimental results and discussion

3.1. Hydrogen adsorption results

The SAXS curve, Fig. 1a, shows four well-defined peaks and a weak fifth peak. This indicates a relatively good quality MCM-41 sample. The d_{10} peak is at 1.72 nm^{-1} corresponding to a distance between pores of 4.21 ± 0.03 nm.

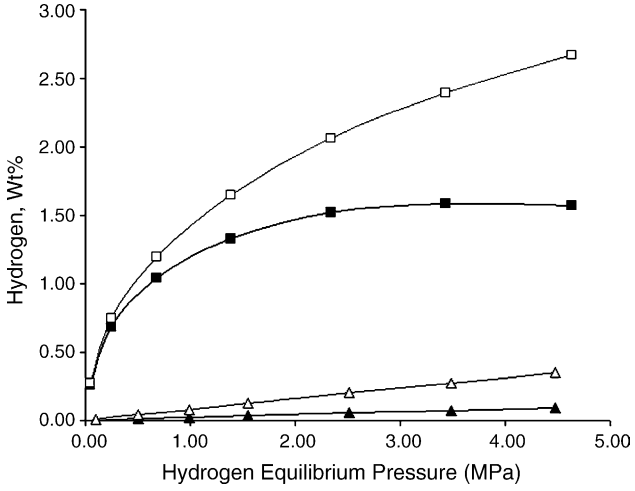

Fig. 2. Hydrogen adsorption on MCM-41. Excess adsorption at 77 K (■), gravimetric adsorption at 77 K (□), excess adsorption at 296 K (△), gravimetric adsorption at 296 K (+).

In the volumetric hydrogen adsorption experiments, the density of the sample was taken as 2.2 g/cm^3. This is the generally accepted value for the density of the walls of MCM-41 though variations have been reported [10]. Assuming a density of 2.2 g/cm^3 infers that the pore volume of the MCM-41 sample is counted as part of the sample cell volume. The resulting hydrogen adsorption is therefore an excess wt%. If the pore volume of the sample (0.73 ml/g as calculated from N_2 adsorption) is included in the volume of the sample then we can derive a gravimetric (where gravimetric wt% is total amount of hydrogen within the pores) wt%. Fig. 2 shows the excess and the gravimetric hydrogen adsorption on our MCM-41 sample at 77 and 296 K. Only the adsorption curve is shown as desorption showed no hysteresis.

The amount of H_2 adsorbed at room temperature (296 K) is low. The excess adsorption is linear and reaches a value of only 0.1 wt% at ∼4.5 MPa. At room temperature the mass of hydrogen stored in an empty sample cell compared to one with adsorbent shows that the adsorbent is less effective than compression alone at all pressures studied.

At 77 K almost all the hydrogen is adsorbed/desorbed instantaneously followed by a gradual pressure change over the period of one minute before equilibrium is reached. The excess weight % capacity at 77 K peaked at 1.6 wt% at a pressure of ∼3.5 MPa. This maximum occurs at a similar pressure to that previously reported on powdered activated carbon samples [11,12]. The gravimetric wt% does not reach a maximum in the pressure range studied (2.7 wt% at ∼4.5 MPa), also similar to previous findings [12]. Comparing the mass of hydrogen in an empty cell at 0.5 bar and 77 K compared to one filled with adsorbent under the same conditions reveals that the presence of adsorbent increases the amount of hydrogen present by a factor of 4. This increase over the mass of hydrogen stored in an empty cell drops to a factor of 1.1 by 4.5 MPa. The MCM-41 sample was lightly compacted into the sample cell for the hydrogenation runs. It has been shown that the structure of MCM-41 remains relatively unchanged after undergoing uniaxial compression at 100 MPa [13]. Consequently, using compressed pellets of MCM-41 as the sample will probably result in a lower wt% of hydrogen but a significant increase in the volumetric storage of hydrogen [12].

Interpolation of the data to a pressure of 1 bar and 77 K yields 0.4 excess wt% of hydrogen. This is marginally lower than the value of 0.58 wt% reported by Nijkamp et al. [14] on a sample of MCM-41 tested at 77 K and 1 bar. Examination of their data reveals that the surface area of their sample is comparable to ours (1017 m^2/g compared to 1006 m^2/g) but that their pore volume (1.04 ml/g) is noticeably larger (0.73 ml/g). Incidentally, the ratio of hydrogen adsorption between the samples and the ratio of pore volumes between the samples are almost identical (0.69 versus 0.70). This indicates a possible link between the pore volume and hydrogen adsorption.

3.2. SAXS modelling results

As shown in Fig. 1a the model intensity calculated by GNOM is in good agreement with the experimental data over the full q-range. In the region where the two data sets overlap the model intensity is in better agreement with intensity recorded at the shorter sample-detector distance. The data recorded at the shorter sample-detector distance shows an increase in peak broadening and decrease in peak height. We expect this to occur since the detector resolution (in the detector plane) is fixed and the detector subtends a greater solid angle at smaller sample-detector distances.

The cross-section correlation function calculated from the experimental data is displayed in Fig. 1b. By assuming a two-phase structure (pore and wall) the following definition and interpretations of $\gamma_c(r)$ can be made; if we choose at random a point within the cross-section, $\gamma_c(r)$ is proportional to the excess probability that a point located a distance r away will lie in the same phase. When there is equal probability that the second point will lie in the same or different phases, $\gamma_c(r) = 0$. With this definition one can understand how the peaks in the CF are approximately located at the nearest neighbour distances of the hexagonal lattice. However, it is not a requirement that a peak must occur in $\gamma_c(r)$ at all nearest neighbour distances since the pores are of a finite size.

Numerical simulations of ideal MCM-41 structures have shown that when the pore size is larger than the wall thickness, as is the case in our sample of MCM-41, the position of the first minimum in $\gamma_c(r)$ can only give a lower limit to the pore size. Theoretically, the exact pore size can be determined by inspection of $\gamma_c(r)$ only if the pore size is smaller than the wall thickness. Simulations have also shown that regardless of the pore size, the position of the first maximum in $\gamma_c(r)$ corresponds to the lattice parameter a. From $\gamma_c(r)$ calculated by GNOM in Fig. 1b, it is estimated that the pore size is $d_p \geq 2.3$ nm and the lattice parameter

$a = 4.0 \pm 0.2$ nm. This is in good agreement with the value of 4.21 ± 0.03 nm determined directly from the position of the d_{10} diffraction peak. The wall thickness, w_t is determined from $w_t = (a - d_p) \leq 1.7$ nm.

4. Conclusion and future work

MCM-41 has been shown to be capable of reversibly absorbing a maximum of 1.6 excess wt% (2.4 gravimetric wt%) of hydrogen at ~3.5 MPa at 77 K. While the excess wt% of hydrogen peaked, the total gravimetric wt% of adsorbed hydrogen continued to increase with pressure as would be expected due to the increasing bulk density of hydrogen. The excess amount adsorbed at room temperature was low at 0.1 wt%. The increase in the amount of hydrogen in a sample cell with adsorbent compared to an empty sample cell dropped from a factor of 4 at ~0.05 MPa to 1.1 at ~4.5 MPa for a sample at 77 K. This study only covered the hydrogen adsorption on what can be considered a typical MCM-41 sample. A number of paths for improving the hydrogen uptake of this material are possible. These include: creating samples with smaller pores and using post-synthesis treatment to increase the pore volume. Compression of MCM-41 into pellets should yield an increase in the volumetric adsorption of hydrogen but at the expense of gravimetric wt%. Preliminary work is also under way on MCM-41 samples doped with different additives. The hydrogen adsorption properties of these samples and their modelling will be presented at a later date. We have shown that the small-angle intensity of MCM-41 can be modelled successfully by the cross-section correlation function. Preliminary interpretations of $\gamma_c(r)$ calculated by GNOM allowed a lower limit of the pore size to be estimated. Future work will be focused on interpreting $\gamma_c(r)$ to elucidate more detailed information about the pore structure.

Acknowledgments

D.S. and C.M. would like to thank the Australian government for the granting of an Australian Post Graduate Award with Stipend (APAWS). C.B. acknowledges the financial support of the Australian Research Council for REIF grant R00107962 2001, which enabled the SAXS studies to be undertaken.

References

[1] A. Zuttel, Mater. Today (2003) 24–33.
[2] J.S. Beck, J.C. Vartuli, W.J. Roth, M.E. Leonowicz, C.T. Kresge, K.D. Schmidt, C.T.-W. Chu, D.H. Olson, E.W. Sheppard, S.B. McCullen, J.B. Higgins, J.L. Schlenker, J. Am. Chem. Soc. 114 (1992) 10834–10843.
[3] H. Hemmes, A. Driessen, R. Griessen, J. Phys. C: Solid State Phys. 19 (1986) 3571–3585.
[4] K.G. Mclennan, E. Gray, Meas. Sci. Technol. 15 (2004) 211–215.
[5] T.C. Huang, H. Torya, T.N. Blanton, Y. Wu, J. Appl. Cryst. 26 (1993) 180–184.
[6] L.A. Feigin, D.I. Svergun, Structure Analysis by Small-angle X-ray and Neutron Scattering, Plenum Press, New York, 1987.
[7] G. Porod, O. Glatter, O. Kratky (Eds.), Small-angle X-ray Scattering, Academic Press, New York, 1982, pp. 17–51.
[8] D.I. Svergun, J. Appl. Cryst. 25 (1992) 495–503.
[9] A.N. Tikhonov, V.Y. Arsenin, Solution of Ill-posed Problems, Wiley, New York, 1977.
[10] N. Floquet, J.P. Coulomb, S. Giorgio, Y. Grillet, P.L. Llewellyn, Stud. Surf. Sci. Catal. 117 (1998) 583–590.
[11] R.K. Agarwal, J.S. Noh, J.A. Schwarz, P. Davini, Carbon 25 (1987) 219–226.
[12] L. Zhou, Y. Zhou, Y. Sun, Int. J. Hydrogen Energy 29 (2004) 319–322.
[13] M. Broyer, S. Valange, J.P. Bellat, O. Bertrand, G. Weber, Z. Gabelica, Langmuir 18 (2002) 5083–5091.
[14] M.G. Nijkamp, J.E.M.J. Raaymakers, A.J. van Dillen, K.P. de Jong, Appl. Phys. A: Mater. Sci. Process. 72 (2001) 619–623.